Pyrolysis and char reactivity of a poor-quality refuse-derived fuel (RDF) from municipal solid waste

Joan J. Manyà [a,], Fernando García-Ceballos [b], Manuel Azuara [c], Nieves Latorre [c], Carlos Royo [c]*

[a] Aragón Institute of Engineering Research (I3A), University of Zaragoza, Spain

[b] Technological College of Huesca, University of Zaragoza, Spain

[c] Institute of Nanoscience of Aragón (INA), University of Zaragoza, Spain

[*] Corresponding author: Joan J. Manyà. E-mail address: joanjoma@unizar.es

1

HIGHLIGHTS

- Increasing both heating rate and peak temperature led to more reactive RDF chars.

- The co-pyrolysis of the RDF and two-phase olive mill waste was also investigated.

- The reactivity of resulting TPOMW chars increased in the presence of RDF.

- The carbonization efficiency of TPOMW was improved in the presence of RDF.

- Results motivate further studies on the use of this RDF as pyrolysis additive.

ABSTRACT

The present study focuses on analyzing the pyrolysis and combustion behaviors of a refuse-derived fuel (RDF), which is generated in a MSW treatment plant located in Zaragoza (Spain). Pyrolysis experiments were carried out in a TGA apparatus and a fixed-bed reactor at different peak temperatures (400 and 600 °C) and heating rates (5 and 40 °C min^{-1}). The reactivity towards oxygen of produced chars was also measured in the same TGA device at a heating rate of 10 °C min^{-1} and a final temperature of 800 °C. Pyrolysis results were significantly affected by peak temperature and heating rate. The found effect of peak temperature on char and fixed-carbon yields as well as on measured properties (H:C and O:C ratios, BET surface area and average pore diameter) was in agreement with previous studies. However, the effect of heating rate, especially on the release rate of volatiles, could be explained by a change in the pyrolysis reactions scheme. The RDF-derived chars obtained at the highest heating rate showed a higher reactivity in air. In addition, an increase in peak temperature also led to a higher reactivity. This result can indicate that the carbon present in the RDF-derived char is dispersed within an ash matrix containing a high number of active sites, the distribution of which could be improved when heating rate (and, to a lesser extent, peak temperature) is increased. The addition of 10 wt. % RDF to two-phase olive mill waste prior to slow pyrolysis led to an apparent increase in the carbonization efficiency as well as to an enhancement of the resultant char's reactivity in air.

KEYWORDS

RDF; MSW; Pyrolysis; Biochar; Reactivity; AAEM species

1. Introduction

According to the hierarchy principle of the EU 2008/98/CE directive [1], the management of municipal solid waste (MSW) should be focused on promoting waste reduction, reuse, recycling and recovery. In other words, MSW treatment processes should be aimed at minimizing disposal practices such as landfilling. In Europe, the mechanical/biological treatment (MBT) of MSW is an increasing option in order to comply with minimization of biodegradable waste landfilling [2] (for EU member countries, the amount of biodegradable material must be reduced to least 35% of the 1995 level by 2016, as requested by the EU 1999/31/EC directive [3]). In MBT processes, a series of biological and mechanical treatments are combined to process waste into recyclables, biogas and/or compost [4]. Combined anaerobic/aerobic treatment of the mechanically separated organic fraction of municipal solid waste (OFMSW) is a particular case of MBT process, which is composed of four main steps [5]: pre-treatment, anaerobic digestion, composting/curing phase and compost refining (see Fig. 1 for more details).

Refuse from the compost refining step generated in an anaerobic digestion and composting plant located in Zaragoza (Spain) was analyzed in the present study as a potential refuse-derived fuel (RDF). In this treatment plant, the gross stabilized material is refined by means of a 20 mm mesh trommel and then by a densimetric table to separate glass, metal, stones and plastics from the final compost. The composting refuse, which is disposed of by landfilling, is about 18% of the total input to the composting unit. Thus, there is a need to reuse this refuse material as a means to comply with the principles outlined in the above-mentioned EU directives.

Despite the fact that the type of material analyzed here has a very poor quality in terms of RDF, mainly due to its high inorganic content, it becomes interesting to investigate its thermal behavior under both inert and oxidative atmospheres with the view to evaluating its potential use as a co-fuel and/or as an additive material in biomass thermochemical processes (e.g., pyrolysis and gasification). Conventional carbonization or slow pyrolysis processes, by means of which the waste is thermally degraded in absence of oxygen at a low heating rate (typically up to 40 °C min⁻

4

[1]) have been used to generate charcoal for many years ago [6]. The yields and properties of the different pyrolysis products (char, oil and gas) strongly depend on the operating conditions (such as peak temperature, usually in the range 400–650 °C) and reactor configuration [7,8]. In the last years, there is an increasing attention on establishing the best operating conditions for the slow pyrolysis of biomass and/or waste in order to obtain a char material with the most appropriate physicochemical properties for its use as biochar (for both soil amendment and carbon storage purposes) [9-15].

It is well-known that the inorganic mineral matter present in biomass and waste, especially alkali and alkaline earth metals (AAEM), can catalyze both biomass decomposition and char-forming secondary reactions during pyrolysis [16]. This catalytic effect was observed in several earlier studies [17-21], in which lower charcoal yields were reported when various biomass feedstocks were leached with hot water as a measure to partially remove inorganic matter. The additional charcoal formation linked to the catalytic role of AAEM is certainly interesting in terms of maximizing the char yield and the fixed-carbon content for both biochar and biofuel purposes.

Biomass-derived chars are usually more reactive than coal chars, mainly due to their lesser ordered structure and higher oxygen content [22,23], as well as the catalytic effect of the inorganic elements [24-26]. Alkali metals, such as Na and especially K are known to be effective catalysts for the oxidation reactions [25]. Furthermore, the AAEM oxides and salts are also active catalysts for steam and CO_2 gasification of carbon [27-29]. As a negative effect that needs to be minimized, these species are also responsible for operational problems (e.g., fouling and slagging) and corrosion of combustion and gasification equipment [30]. In summary, the inherent AAEM species present in the RDF can play an interesting role in both pyrolysis step and subsequent char combustion/gasification step, in spite of the fact that the secondary char, the formation of which is promoted by AAEM species, is usually less porous and thus less accessible to gaseous reactants [8,22].

The present study aims to analyze, at first, the slow pyrolysis behavior (under both TGA and fixed-bed conditions) of the RDF samples as a function of both peak temperature (i.e., highest temperature value) and heating rate. The resulting chars were then submitted to an oxidation step to analyze their reactivity as a function of pyrolysis conditions. As literature does not provide a clear picture regarding the relationship between pyrolysis conditions and char reactivity [23,31], results reported here will provide useful information to guide further studies. Finally, the effect of adding a relatively small fraction of RDF to a given biomass feedstock (two-phase olive mill waste, TPOMW) on char yield and properties, as well as on char reactivity in air, is also examined.

2. Materials and methods

2.1. Materials

The as-received refuse material (RDF) was crushed and then sieved. The fraction in the range 0.15–1.2 mm was collected and characterized in terms of proximate and elemental analyses. Proximate analyses were performed in quadruplicate according to ASTM standards (D3173 for moisture, D3174 for ash, and D3175 for volatile matter), whereas elemental analyses were carried out using a Leco TruSpec Micro CHNS analyzer (Leco Corporation, USA). In addition, an ADVANT'XP+ XRF spectrometer (Thermo ARL, Switzerland) was used to measure the ash composition on the basis of the weight fractions of the equivalent oxides (according to ASTM standard D4326-04). Table 1 lists the results from the above-mentioned analyses.

As mentioned before, two-phase olive mill waste (TPOMW) as well as a mixture of TPOMW and RDF (dry mixed in a weight ratio TPOMW/RDF of 9/1) were used in the present study to analyze the effect of AAEM species contained in RDF on both pyrolysis and combustion behaviors. The TPOMW samples, which were supplied by an olive oil factory located in the Spanish region of Aragón, were sieved to obtain a particle size in the range of 0.15−1.0 mm. The

moisture and ash contents are 16.85% and 2.27%, respectively. The complete characterization results for TPOMW samples are available in a previous publication [13].

2.2. Char production

Pyrolysis tests were conducted in an atmospheric thermobalance (a MK2 microbalance with a readability of 0.1 μg from CI Precision, UK) under nitrogen atmosphere (with a flow rate through the reaction chamber of 200 cm^3 NTP min^{-1}). An unreplicated 2-level factorial design was adopted to study the effect of two factors: peak temperature (400–600 °C) and linear heating rate (5–40 °C min^{-1}). Three replicates at the center point (22.5 °C min^{-1} and 500 °C) were performed to simultaneously estimate the experimental error and the overall curvature effect [32,33]. Table 2 shows the matrix of the experimental design. The initial sample weight was 250 mg, a relatively large amount compared to the most commonly used initial sample masses (1–4 mg), which are preferred to avoid serious systematic errors in the measurement of the sample temperature in a TGA device [16]. However, using small sample sizes can also lead to other potential problems, such as the inability to asses a representative sample and the possibility to magnify surface phenomena at the expense of intra-bed controlling processes [34].

Additional pyrolysis tests at peak temperatures of 400 and 600 °C were conducted in a fixed-bed reactor in order to determine the effect of reducing the diffusion rate of volatiles on the char yield. In other words, the contact time between volatiles and the solid matrix is much longer in a fixed-bed device than it is in a TGA apparatus, leading to an enhancement of secondary charring reactions. Fixed-bed pyrolysis runs were performed by duplicate for both TPOMW and TPOMW-RDF mixtures using a column made of borosilicate glass (total available length: 150 mm; inner diameter: 25 mm). The initial mass of solid was around 8 g. The fixed-bed temperature was controlled by means of a cylindrical electric furnace connected to a PID controller. The same heating rates than those used in the TGA apparatus (5 and 40 °C min^{-1}) were selected. A holding time at the peak temperature of 30 min was maintained.

2.3. Char characterization

The surface area of the produced chars was analyzed by means of N_2 physisorption at -196 °C on a TriStar 3000 gas adsorption analyzer (Micromeritics, USA). Surface area (S_{BET}) was calculated using the Brunauer–Emmet–Teller (BET) model from adsorption data obtained at relatively low relative pressures (0.05–0.20). The total pore volume (V_t) was determined from the specific adsorption of N_2 at a $p/p_0 = 0.99$. The t-plot method was used to estimate the external surface area (S_{ext}), whereas the micropore surface area (S_{mic}) was calculated as the difference between S_{BET} and S_{ext} [35]. The average pore diameter (d_{avg}) was calculated from V_t and S_{BET}.

In addition, the pore size distribution of meso- and macropores was determined using a mercury intrusion porosimetry (MIP) analyzer (AutoPore IV 9500 from Micromeritics, USA). For each sample, a cycle of mercury intrusion and extrusion in a pressure range from 0.00351 to 414 MPa was performed, which covered a pore size range from 3 nm to 360 μm. The total meso- and macropore surface area (S_{tot}) was calculated assuming the Washburn's model [36].

The obtained chars were also characterized by proximate, elemental and XRF analyses according to the same procedures described in Sec. 2.1.

2.4. Char combustion

Combustion tests were conducted for each char (using the same TGA device described above) at a constant heating rate of 10 °C min^{-1}, a final temperature of 800 °C and an initial sample mass of 25 mg. A mixture of air and N_2 (at a volumetric ratio air/N_2 of 1:4) was passed through the reaction chamber at a flow rate of 200 cm^3 NTP min^{-1}. In order to estimate the sample mass loss due to the release of volatiles from char, the same tests were replicated under a pure N_2 atmosphere keeping constant the rest of conditions.

3. Results and discussion

3.1. RDF-derived char production through slow pyrolysis

Differential thermogravimetric curves for the vertex points (runs 2, 3, 4 and 6) are displayed together in Fig. 2. With the aim to make consistent comparisons among runs plotted in Fig. 2 (conducted at different heating rates), values on the y-axis correspond to the time derivative of the ash-free normalized sample mass (m_{af}) multiplied by β^{-1}; m_{af} was calculated as follows:

$$m_{af} = \frac{(m_t / m_0)}{(1 - x_{ash})} \tag{1}$$

where m_t is the sample mass, m_0 is the initial sample mass, and x_{ash} is the mass fraction of ash in the raw material.

From Fig. 2 it can be observed that two peaks appeared for runs conducted at a peak temperature of 600 °C: a major peak between 200 and 375 °C and a minor one between 400 and 500 °C. The major peak should be attributed to the biogenic fraction, which is mainly composed of lignocellulosic structures (from paper, cardboard, textil, wood, etc.) [31,37]. For its part, the minor peak could correspond to the degradation of plastics (such as low-density polyethylene, high-density polyethylene and polypropylene) [37-39]. An interesting finding is the fact that the highest devolatilzation rate for tests conducted at 40 °C min^{-1} was reached at a lower temperature, in comparison with the case of the samples pyrolyzed at 5 °C min^{-1} (around 280 °C and 305 °C, respectively). Usually, pyrolysis profiles shift to a higher temperature region when heating rate is increased, due to the fact that the heat required for devolatilization is reached later at higher temperatures (i.e., heat transfer limitations) [40-45]. Thus, the observed result suggests that an increase from 5 to 40 °C min^{-1} could lead to a faster release of volatiles, probably induced by an increase in the thermal driving force coupled to a higher catalytic activity of the AAEM species. Simultaneously, a fraction of these volatiles may undergo exothermic secondary charring reactions at lower temperatures leading to important changes in thermal profiles.

Table 3 displays the main results obtained from the factorial design of experiments (which is summarized in Table 2). The following response variables were evaluated: the mass yield of char in a dry basis (y_{char}), the fixed-carbon yield (y_{FC}) in a dry and ash-free basis and calculated

9

according to Eq. (2), and several char properties (the molar H:C and O:C ratios deduced from elemental analyses, the BET and micropore surface areas estimated from the N_2 adsorption/desorption isotherms, and the total meso- and macropore surface area from MIP measurements).

$$y_{FC} = \left(\frac{m_{char}}{m_{raw}} \right) \left(\frac{\%FC}{100 - \%ash} \right) \tag{2}$$

In Eq. (2), *%FC* and *%ash* are the percentage of fixed-carbon present in the char and the percentage of ash in the raw material, respectively; whereas the ratio between m_{char} (mass of produced char) and m_{raw} (dry mass of raw material) is equal to the char yield (y_{char}). It is now well accepted that the y_{FC} value is a better indicator of the efficiency of the pyrolytic conversion than y_{char} [13,14,46]. Furthermore, and as reported in earlier studies [9,13,14], the fixed-carbon content (and, in certain cases, the fixed-carbon yield) is usually correlated with the molar H:C and O:C ratios as well as with the percentage of aromatic carbon. In other words, the fixed-carbon content and, to a lesser extent, the y_{FC} value can also be taken as rough indicators of the potential stability of a given char in soil environments.

For each response variable, a regression model including the linear and linear interaction terms was estimated. Functional relationships between the response (*y*) and the coded independent variables (x_1, for peak temperature and x_2, for heating rate) are quantified by means of the estimated parameters of the regression model:

$$y = \beta_0 + \beta_1 x_1 + \beta_2 x_2 + \beta_{12} x_1 x_2 + \varepsilon \tag{3}$$

where β_0, β_j and β_{ij} are the intercept, linear and interaction coefficients; respectively. Statistical significance of model terms was assessed by parametric tests (*t*-test). In the event that the overall curvature term is found to be significant (i.e., *p*-value < 0.05), the linear regression model is not fine enough and a second-order regression model with pure quadratic terms is probably required. Results of the statistical analyses are summarized in Table 4.

As can be seen from Table 4, peak temperature was the only factor that significantly affected both the char and fixed-carbon yields. As expected and consistent with previous studies conducted with different biomass feedstocks [11,13,15,47], an increase in T_{peak} leads to a decrease in y_{char} and an increase in y_{FC}. For the rest of response variables (molar H:C and O:C ratios, S_{BET}, d_{avg} and S_{tot}), the two analyzed factors showed significant main effects. A non-negligible interaction effect was also found for molar H:C and O:C ratios and S_{tot}. For those variables having curvature terms statistically significant (molar H:C and O:C ratios, d_{avg} and S_{tot}), further central composite designs of experiments will be required to find more accurate regression models (i.e., second-order response surface models). In summary, we may conclude from the statistical analysis that working at the highest values of peak temperature and heating rate leads to more potentially stable chars (higher y_{FC} and lower H:C and O:C ratios) with a better developed micro- and mesoporosity at the expense of macroporosity (i.e., higher S_{BET} and lower S_{tot}).

The observed increase in surface area with peak temperature is in good agreement with previous studies. For instance, Jiménez-Cordero et al. [48] reported a marked increase in BET surface area when peak temperature was increased from 400 to 600 °C during pyrolysis of grape seeds. This finding could be related to the fact that temperatures lower than 600 °C induce incomplete devolatilization, which affects the development of porosity. Regarding the effect of heating rate on porosity (less significant than T_{peak} for the S_{BET} variable, as shown in Table 4), Angin [49] reported a decrease in surface area as heating rate increased from 10 to 50 °C min^{-1} when a cake of safflower seed was pyrolyzed at peak temperatures of 400 and 600 °C. The author attributes this result to mass transfer limitations at higher heating rates (i.e., the time for the release of volatiles is shorter and it may lead to an accumulation of volatiles between and within the particles). However, as previously discussed for the thermogravimetric curve given in Fig. 2, an increase in heating rate could lead to a faster release of volatiles, due to a higher driving force coupled to a higher catalytic activity of the AAEM species. Thus, the caused increase in

devolatilization rate at lower temperatures could facilitate the release of volatiles during the course of the process.

As expected, due to the high ash content of the RDF samples and the relatively low pyrolysis temperature, the surface area values listed in Table 3 are relatively modest. For instance, Burhenne et al. [23] reported S_{BET} values ranging from 196 to 397 m^2 g^{-1} for spruce wood-derived chars obtained at a peak temperature of 500 °C. Nevertheless, Lee et al. [50] and Wang et al. [51] observed that the S_{BET} values for chars produced also at a highest temperature of 500 °C exhibited a wide variability depending on the biomass feedstock (14–202 m^2 g^{-1} [50]; 0.17–240 m^2 g^{-1} [51]).

3.2. Effect of RDF addition on the fixed-bed pyrolysis of TPOMW

Fig. 3 compares the mass yields (char yield and fixed-carbon yield) obtained for TPOMW and TPOMW-RDF mixtures. The reported values correspond to the average values from duplicate experiments (standard deviations lower than 2.5%). In order to analyze whether the effects might be purely additive or synergistic, mass char yields were calculated in a dry and ash-free basis ($y_{char,daf}$). From the data displayed in Fig. 3 for $y_{char,daf}$, it seems reasonably clear that there are synergistic effects, the sign of which depends on peak temperature. At 400 °C, the yield of char decreases by the addition of 10% RDF, whereas at 600 °C the opposite trend is observed. This finding could be explained by the fact that, at lower temperature, the higher release of volatiles during the primary devolatilization catalyzed by the AAEM species is not compensated by an equal increase in the formation of secondary char. At this point, it is interesting to compare our results with earlier studies. For instance, Di Blasi et al. [52] reported a marked increase in char yield (40% higher) during pyrolysis of fir wood impregnated with KOH (concentration in wood below 1%) at a peak temperature of 527 °C. More recently, Veksha et al. [53] observed that the addition of 0.24% and 0.48% of KOH during the co-pyrolysis of mixtures of bio-oil and biomass (aspen wood) at 600 °C led to an increase in the mass yield of biochar of 22.3% and 25.2%, respectively. The effect of peak temperature was analyzed by Hayashi et al. [54] during the pyrolysis of mixtures of wood and PVC catalyzed by alkaline and alkaline earth metal hydroxides.

12

One of the major findings reported in the study by Hayashi et al. [54] was that the increase in char yield was affected by peak temperature. More in detail and in line with the results reported here, the addition of hydroxides at temperatures of 300 and 400 °C led to a decrease in char yield.

With regard to the carbonization efficiency (i.e., y_{FC}), the addition of RDF seems to favor carbonization in the main of cases, except for the fixed-bed pyrolysis run conducted until 400 °C at 5 °C min^{-1}. In general, higher y_{FC} values were obtained with the lowest heating rate for both starting materials. A possible explanation for this result is the fact that the higher devolatilization (i.e., lower y_{char}) at the higher heating rate is not accompanied by a proportional increase in the fixed-carbon content of produced chars.

As can also be deduced from the results displayed in Fig. 3, the addition of 10% RDF to TPMOW feedstock led to a certain increase in the BET specific surface area of resultant chars. This increase was more pronounced when pyrolysis of TPOMW was conducted at 40 °C min^{-1} until 600 °C. This finding could be explained by the role played by the AAEM species contained in the RDF material. At any heating rate, the AAEM species catalyze the volatile production from the primary pyrolysis reactions. However, at higher heating rates, the residence time of the pyrolysis vapors inside the biomass particle and through the bed is reduced, leading to less time for catalyzed secondary reactions to take place (the product of which is a less porous char). I should also be noted the BET specific surface areas measured here are very low compared to those reported for other biomass sources at similar peak temperatures [48,50]. Further pyrolysis experiments at temperatures higher than 600 °C would probably be required to obtain chars with higher specific surface areas. In fact, Pellera and Gidarakos [55] observed a remarkably increase in the BET specific surface area when the peak temperature raised from 400 to 700 °C (1.76 and 72.8 m^2 g^{-1}, respectively) during the slow pyrolysis of a Greek olive pomace (a feedstock very similar to that used in the present study).

Concerning the molar H:C and O:C ratios of produced chars as well as their correlation (or lack of it) with both the fixed-carbon yield and fixed-carbon content (in an ash-free basis), Table 5

presents the Pearson's correlation matrix for these variables. It is interesting to highlight that both H:C and O:C ratios were significantly correlated with the fixed-carbon content (Fig. 4 also shows these relationships in a graphical manner), but were not correlated with y_{FC}. As the H:C molar ratio may be considered as a reasonable indicator of the average size of the aromatic clusters in the char [10,11], it seems appropriate to choose this variable, instead of y_{FC}, as a measure of the potential char stability in the soil. Based on this criterion and the information given in Fig. 4, we may conclude that the addition of 10% RDF to TPMOW does not apparently lead to potentially more stable chars, given the similarity in H:C ratios between the pure TPOMW-derived chars and those obtained from the TPOMW-RDF mixture. In any case, all of the chars produced at a peak temperature of 600 °C exhibited low H:C ratios (less than 0.4). According to recommendations from Enders at al. [9], these high temperature chars would have a high carbon sequestration potential.

3.3. RDF-derived char reactivity in air

In order to provide a more comprehensive comparison among RDF-derived chars obtained under different pyrolysis conditions, mass data collected from the TGA apparatus were recalculated in a volatile and ash-free (vaf) basis according to the following equation:

$$m_{vaf} = \frac{\left[m_{air} - (1 - m_{nitro})\right]}{(1 - x_{ashC})} \tag{4}$$

where m_{vaf} is the normalized mass of char in a vaf basis, m_{air} corresponds to the normalized mass (m_t/m_0) obtained under an air atmosphere (i.e, char combustion tests), m_{nitro} is the normalized mass for tests conducted under a N_2 atmosphere (i.e., char pyrolysis tests conducted under the same operating conditions), and x_{ashC} is the mass fraction of ash in the given char. With this procedure, the mass loss due to volatiles release (the content of which in the char is strongly dependent on the pyrolysis peak temperature) is not considered as part of the char reactivity towards oxygen.

Fig. 5a presents the derivative weight curve in a volatile and ash-free basis (DTG_{vaf}), whereas Fig. 5b shows the specific reactivity (R) towards oxygen as a function of char conversion. R was calculated as follows:

$$R = -\frac{dm_{vaf}}{dt}\frac{1}{(m_{air} - m_{air,f})} \tag{5}$$

where $m_{air,f}$ is the final normalized mass (i.e., measured value at the final temperature of 800 °C).

From both graphs it is clear that reactivity strongly depends on pyrolysis conditions. The most reactive chars were those obtained at the highest heating rate (40 °C min^{-1}). Thus, this factor seems to be more influencing than peak temperature for the range of operating conditions used in the present study. In this sense, an increase in heating rate could lead to higher disordered carbon structures, as recently suggested by Zeng et al. [56]. For its part, increasing pyrolysis peak temperature did not result in a decrease in reactivity; on the contrary, high-temperature chars exhibited a slightly higher reactivity, especially for those produced at the lowest heating rate. This finding seems to be in disagreement with previous studies [8,57], in which a decrease in reactivity towards oxygen with peak temperature was reported for chars derived from lignocellulosic precursors (wood spruce and flax straw). In these studies, it was suggested that higher pyrolysis temperatures led to more ordered structures and a higher formation of secondary char (which can cause clogging of pores).

It should also be mentioned that the reactivity of chars did not seem to be only explained by differences in BET surface areas. For instance, the char obtained at 400 °C and 40 °C min^{-1} was very reactive despite its relatively low S_{BET} value. This result may suggest that the carbon present in the RDF-derived char is dispersed within an ash matrix containing a high number of active sites. This possible reason was previously advocated by Dennis et al. [58] to explain the high reactivity of sewage sludge-derived chars, which also had high ash contents and relatively low specific surface areas in comparison with biomass-based low-ash activated carbons. Thus,

increasing heating rate and, to a lesser extent, peak temperature during pyrolysis can lead to a better distribution of the active sites within the ash matrix.

3.4. Effect of RDF addition on the reactivity of the resultant chars

In general and as can be seen in Fig. 6, the reactivity of TPOMW-derived chars was increased in the presence of RDF. The exception was only for the chars obtained at 400 °C and 40 °C min^{-1}, where similar reactivities were observed. However, for the chars produced at 600 °C and 40 °C min^{-1}, the increase in reactivity was particularly high. This apparent discrepancy in the results could be due to multiple reasons. First, a certain degree of heterogeneity among the different samples is difficult to avoid in practice; this fact can result in different degrees of distribution of the inorganic matter on the TPOMW particles. Second, the surface area of low-temperature TPOMW-derived chars could be excessively small to allow a rapid diffusion of oxygen. Further studies including the morphological characterization of chars are needed to provide a more detailed analysis.

Another aspect that should be considered in further studies is the volatilization of AAEM species and their chemical speciation during pyrolysis. In this sense, in a recent study [59] it is highlighted that the majority of the volatilization of K and Na occurs between 600 °C and 700 °C (at temperatures higher than that used in the present study). On the other hand, the high content of Ca in the RDF (see Table 1) suggests that this cation could play a dominant catalytic role during the char combustion. In fact, Zhang et al. [60] already observed a good correlation between calcium concentration and the reactivity towards oxygen of manure-derived chars (obtained through slow pyrolysis at a peak temperature of 700 °C).

4. Conclusions

Based on the results of the present study, the following conclusions can be drawn:

(1) Pyrolysis of the RDF used here is greatly affected by peak temperature and heating rate. The found effect of peak temperature on char and fixed-carbon yields as well as on measured

properties is in agreement with previous studies. However, the effect of heating rate, especially on the release rate of volatiles, could be related to a change in the pyrolysis reactions scheme. Further studies are needed to clarify this point.

(2) The addition of 10% RDF to TPMOW feedstock prior to slow pyrolysis leads to an apparent increase in the carbonization efficiency. This finding motivates further studies to evaluate the co-pyrolysis of this type of RDF and biomass feedstocks as a way to simultaneously manage the waste and increase the production yield of biomass-based chars.

(3) The RDF-derived chars obtained at the highest heating rate (40 °C min^{-1}) have a higher reactivity towards oxygen than those produced at 5 °C min^{-1}. In addition, increasing the peak temperature also has a positive effect on char reactivity. This result can indicate that the carbon present in the RDF-derived char is dispersed within an ash matrix containing a high number of active sites, the distribution of which is improved when the heating rate (and, to a lesser extent, the peak temperature) is increased.

(4) Due to the catalytic effect of inorganic components contained in the RDF, an enhancement of the TPOMW-derived char reactivity in air by addition of 10% RDF has been observed. Thus, exploring the use of MSW-derived RDFs to produce high-quality solid biofuels for more efficient combustion might be of special interest to the research community.

Nomenclature

d_{avg} = average pore diameter (nm)

m_0 = initial sample mass for TGA experiments (mg)

m_{af} = ash-free normalized sample mass for TGA experiments (–)

m_{air} = normalized sample mass for TGA experiments conducted in a diluted air atmosphere (–)

1     $m_{air,f}$ = final value of m_{air} (–)

2   m_{char} = mass of produced char (g)

3   m_{nitro} = normalized sample mass for TGA experiments conducted in a N_2 atmosphere (–)

4   m_{raw} = dry mass of raw material (g)

5   m_t = sample mass at a given time for TGA experiments (mg)

6   m_{vaf} = normalized sample mass in a volatile- and ash-free (vaf) basis for TGA experiments (–)

7   R = intrinsic reactivity towards oxygen (min^{-1})

8   R^2_{adj} = adjusted coefficient of determination

9   S_{BET} = Brunauer–Emmet–Teller specific surface area ($m^2\ g^{-1}$)

10   S_{ext} = external surface area ($m^2\ g^{-1}$)

11   S_{mic} = micropore surface area ($m^2\ g^{-1}$)

12   S_{tot} = total meso- and macropore area ($m^2\ g^{-1}$)

13   T_{peak} = pyrolysis peak temperature (°C)

14   V_t = total pore volume ($cm^3\ g^{-1}$)

15   x_1 = coded variable for peak temperature

16   x_2 = coded variable for heating rate

17   x_{ash} = mass fraction of ash in the raw material (–)

18   x_{ashC} = mass fraction of ash in the produced char (–)

19   y_{char} = biochar yield in a dry basis (–)

20     $y_{char,daf}$ = biochar yield in a daf basis (–)

21   y_{FC} = fixed-carbon yield in a dry and ash-free basis (–)

22   *Greek Symbols*

23   β = heating rate (°C min^{-1})

24   β_0 = regression coefficient for the intercept term

25   β_1 = regression coefficient for the linear effect of peak temperature

26   β_2 = regression coefficient for the linear effect of heating rate

1   β_{12} = regression coefficient for the interaction term

2   *Acronyms*

3   AAEM = alkali and alkaline Earth metals

4   BET = Brunauer Emmett Teller

5   DTG = differential thermogravimetric analysis

6   FC = fixed carbon

7   MBT = mechanical and biological treatment

8   MIP = mercury intrusion porosimetry

9   MSW = municipal solid waste

10   OFMSW = organic fraction of municipal solid waste

11   PID = proportional integral derivative

12   RDF = refuse-derived fuel

13   TGA = thermogravimetric analysis

14   TPOMW = two-phase olive mill waste

15   XRF = X-ray fluorescence

16

References

[1] The European Union, Directive 2008/98/EC of the European Parliament and of the Council of 19 November 2008 on waste and repealing certain Directives. L 312 (2008) 3-30.

[2] E.C. Rada, G. Andreottola, RDF/SRF: Which perspective for its future in the EU, Waste Manage. 32 (2012) 1059-1060.

[3] The Eurpean Union, Directive 1999/31/EC of the Council of the European Union of 26 April 1999 on the landfill of waste. L 182 (1999) 1-19.

[4] S.T. Wagland, P. Kilgallon, R. Coveney, A. Garg, R. Smith, P.J. Longhurst, et al., Comparison of coal/solid recovered fuel (SRF) with coal/refuse derived fuel (RDF) in a fluidised bed reactor, Waste Manage. 31 (2011) 1176-1183.

[5] M. Pognani, R. Barrena, X. Font, A. Sánchez, A complete mass balance of a complex combined anaerobic/aerobic municipal source-separated waste treatment plant, Waste Manage. 32 (2012) 799-805.

[6] J.J. Manyà, Pyrolysis for Biochar Purposes: A Review to Establish Current Knowledge Gaps and Research Needs, Environ. Sci. Technol. 46 (2012) 7939-7954.

[7] M.J. Antal, M. Gronli, The Art, Science, and Technology of Charcoal Production, Ind. Eng. Chem. Res. 42 (2003) 1619-1640.

[8] J. Recari, C. Berrueco, S. Abelló, D. Montané, X. Farriol, Effect of temperature and pressure on characteristics and reactivity of biomass-derived chars, Bioresour. Technol. 170 (2014) 204-210.

[9] A. Enders, K. Hanley, T. Whitman, S. Joseph, J. Lehmann, Characterization of biochars to evaluate recalcitrance and agronomic performance, Bioresour. Technol. 114 (2012) 644-653.

[10] H. Sun, W.C. Hockaday, C.A. Masiello, K. Zygourakis, Multiple Controls on the Chemical and Physical Structure of Biochars, Ind Eng Chem Res. 51 (2012) 3587-3597.

[11] F. Ronsse, S. van Hecke, D. Dickinson, W. Prins, Production and characterization of slow pyrolysis biochar: influence of feedstock type and pyrolysis conditions, GCB Bioenergy. 5 (2013) 104-115.

[12] O. Mašek, P. Brownsort, A. Cross, S. Sohi, Influence of production conditions on the yield and environmental stability of biochar, Fuel. 103 (2013) 151-155.

[13] J.J. Manyà, S. Laguarta, M.A. Ortigosa, J.A. Manso, Biochar from Slow Pyrolysis of Two-Phase Olive Mill Waste: Effect of Pressure and Peak Temperature on its Potential Stability, Energy Fuels. 28 (2014) 3271-3280.

[14] J.J. Manyà, M.A. Ortigosa, S. Laguarta, J.A. Manso, Experimental study on the effect of pyrolysis pressure, peak temperature, and particle size on the potential stability of vine shoots-derived biochar, Fuel. 133 (2014) 163-172.

[15] A. Budai, L. Wang, M. Gronli, L.T. Strand, M.J. Antal, S. Abiven, et al., Surface Properties and Chemical Composition of Corncob and Miscanthus Biochars: Effects of Production Temperature and Method, J. Agric. Food Chem. 62 (2014) 3791-3799.

[16] J.E. White, W.J. Catallo, B.L. Legendre, Biomass pyrolysis kinetics: A comparative critical review with relevant agricultural residue case studies, J. Anal. Appl. Pyrolysis. 91 (2011) 1-33.

[17] H. Teng, Y.C. Wei, Thermogravimetric Studies on the Kinetics of Rice Hull Pyrolysis and the Influence of Water Treatment, Ind. Eng. Chem. Res. 37 (1998) 3806-3811.

[18] P.A. Jensen, F.J. Frandsen, K. Dam-Johansen, B. Sander, Experimental Investigation of the Transformation and Release to Gas Phase of Potassium and Chlorine during Straw Pyrolysis, Energy Fuels. 14 (2000) 1280-1285.

[19] J.J. Manyà, E. Velo, L. Puigjaner, Kinetics of biomass pyrolysis: A reformulated three-parallel-reactions model, Ind Eng Chem Res. 42 (2003) 434-441.

[20] C.J. Gomez, J.J. Manyà, E. Velo, L. Puigjaner, Further applications of a revisited summative model for kinetics of biomass pyrolysis, Ind Eng Chem Res. 43 (2004) 901-906.

[21] E. Meszaros, E. Jakab, G. Varhegyi, P. Szepesvary, B. Marosvolgyi, Comparative study of the thermal behavior of wood and bark of young shoots obtained from an energy plantation, J Anal. Appl. Pyrolysis. 72 (2004) 317-328.

[22] C. Di Blasi, Combustion and gasification rates of lignocellulosic chars, Prog Energy Combust Sci. 35 (2009) 121-140.

[23] L. Burhenne, J. Messmer, T. Aicher, M. Laborie, The effect of the biomass components lignin, cellulose and hemicellulose on TGA and fixed bed pyrolysis, J. Anal. Appl. Pyrolysis. 101 (2013) 177-184.

[24] C. Dupont, T. Nocquet, J.A. Da Costa Jr., C. Verne-Tournon, Kinetic modelling of steam gasification of various woody biomass chars: Influence of inorganic elements, Bioresour. Technol. 102 (2011) 9743-9748.

[25] P. Lahijani, Z.A. Zainal, A.R. Mohamed, M. Mohammadi, CO2 gasification reactivity of biomass char: Catalytic influence of alkali, alkaline earth and transition metal salts, Bioresour. Technol. 144 (2013) 288-295.

[26] S.G. Sahu, N. Chakraborty, P. Sarkar, Coal–biomass co-combustion: An overview, Renewable Sustainable Energy Rev. 39 (2014) 575-586.

[27] J.M. Encinar, J.F. González, J.J. Rodríguez, M.J. Ramiro, Catalysed and uncatalysed steam gasification of eucalyptus char: influence of variables and kinetic study, Fuel. 80 (2001) 2025-2036.

[28] H. Wu, K. Yip, Z. Kong, C. Li, D. Liu, Y. Yu, et al., Removal and Recycling of Inherent Inorganic Nutrient Species in Mallee Biomass and Derived Biochars by Water Leaching, Ind Eng Chem Res. 50 (2011) 12143-12151.

[29] P. Nanou, H.E. Gutiérrez Murillo, W.P.M. van Swaaij, G. van Rossum, S.R.A. Kersten, Intrinsic reactivity of biomass-derived char under steam gasification conditions-potential of wood ash as catalyst, Chem. Eng. J. 217 (2013) 289-299.

[30] S. Fournel, J.H. Palacios, R. Morissette, J. Villeneuve, S. Godbout, M. Heitz, et al., Influence of biomass properties on technical and environmental performance of a multi-fuel boiler during on-farm combustion of energy crops, Appl. Energy. 141 (2015) 247-259.

[31] R.B. Silva, S. Martins-Dias, C. Arnal, M.U. Alzueta, M. Costa, Pyrolysis and Char Characterization of Refuse-Derived Fuel Components, Energy Fuels. 29 (2015) 1997-2005.

[32] D.C. Montgomery, Design and analysis of experiments, 6th ed. John Wiley & Sons, Hoboken, NJ, 2005.

[33] J.J. Manyà, F.X. Roca, J.F. Perales, TGA study examining the effect of pressure and peak temperature on biochar yield during pyrolysis of two-phase olive mill waste, J. Anal. Appl. Pyrolysis. 103 (2013) 86-95.

[34] G. Varhegyi, B. Bobaly, E. Jakab, H. Chen, Thermogravimetric Study of Biomass Pyrolysis Kinetics. A Distributed Activation Energy Model with Prediction Tests, Energy Fuels. 25 (2011) 24-32.

[35] W. Hao, E. Björkman, M. Lilliestråle, N. Hedin, Activated carbons prepared from hydrothermally carbonized waste biomass used as adsorbents for CO2, Appl. Energy. 112 (2013) 526-532.

[36] S.P. Rigby, R.S. Fletcher, J.H. Raistrick, S.N. Riley, Characterisation of porous solids using a synergistic combination of nitrogen sorption, mercury porosimetry, electron microscopy and micro-focus X-ray imaging techniques, Phys. Chem. Chem. Phys. 4 (2002) 3467-3481.

[37] E.C. Efika, J.A. Onwudili, P.T. Williams, Products from the high temperature pyrolysis of RDF at slow and rapid heating rates, J. Anal. Appl. Pyrolysis. 112 (2015) 14-22.

[38] L. Sørum, M.G. Grønli, J.E. Hustad, Pyrolysis characteristics and kinetics of municipal solid wastes, Fuel. 80 (2001) 1217-1227.

[39] D. Montané, S. Abelló, X. Farriol, C. Berrueco, Volatilization characteristics of solid recovered fuels (SRFs), Fuel Process Technol. 113 (2013) 90-96.

[40] T. Mani, P. Murugan, J. Abedi, N. Mahinpey, Pyrolysis of wheat straw in a thermogravimetric analyzer: Effect of particle size and heating rate on devolatilization and estimation of global kinetics, Chem. Eng. Res. Design. 88 (2010) 952-958.

[41] Z. Shuping, W. Yulong, Y. Mingde, L. Chun, T. Junmao, Pyrolysis characteristics and kinetics of the marine microalgae Dunaliella tertiolecta using thermogravimetric analyzer, Bioresour. Technol. 101 (2010) 359-365.

[42] D. Vamvuka, S. Sfakiotakis, Effects of heating rate and water leaching of perennial energy crops on pyrolysis characteristics and kinetics, Renewable Energy. 36 (2011) 2433-2439.

[43] A. Skreiberg, Ø Skreiberg, J. Sandquist, L. Sørum, TGA and macro-TGA characterisation of biomass fuels and fuel mixtures, Fuel. 90 (2011) 2182-2197.

[44] B.L.F. Chin, S. Yusup, A. Al Shoaibi, P. Kannan, C. Srinivasakannan, S.A. Sulaiman, Kinetic studies of co-pyrolysis of rubber seed shell with high density polyethylene, Energy Conversion Manage. 87 (2014) 746-753.

[45] J.J. Manyà, S. Laguarta, M.A. Ortigosa, Study on the Biochar Yield and Heat Required during Pyrolysis of Two-Phase Olive Mill Waste, Energy Fuels. 27 (2013) 5931-5939.

[46] M.J. Antal, S.G. Allen, X. Dai, B. Shimizu, M.S. Tam, M. Gronli, Attainment of the Theoretical Yield of Carbon from Biomass, Ind. Eng. Chem. Res. 39 (2000) 4024-4031.

[47] K. Crombie, O. Masek, S.P. Sohi, P. Brownsort, A. Cross, The effect of pyrolysis conditions on biochar stability as determined by three methods, GCB Bioenergy. 5 (2013) 122-131.

[48] D. Jimenez-Cordero, F. Heras, N. Alonso-Morales, M.A. Gilarranz, J.J. Rodriguez, Porous structure and morphology of granular chars from flash and conventional pyrolysis of grape seeds, Biomass Bioenergy. 54 (2013) 123-132.

[49] D. Angın, Effect of pyrolysis temperature and heating rate on biochar obtained from pyrolysis of safflower seed press cake, Bioresour. Technol. 128 (2013) 593-597.

[50] Y. Lee, J. Park, C. Ryu, K.S. Gang, W. Yang, Y. Park, et al., Comparison of biochar properties from biomass residues produced by slow pyrolysis at 500 °C, Bioresour. Technol. 148 (2013) 196-201.

[51] Y. Wang, Y. Hu, X. Zhao, S. Wang, G. Xing, Comparisons of Biochar Properties from Wood Material and Crop Residues at Different Temperatures and Residence Times, Energy Fuels. 27 (2013) 5890-5899.

[52] C. Di Blasi, A. Galgano, C. Branca. Effects of Potassium Hydroxide Impregnation on Wood Pyrolysis, Energy Fuels. 23 (2009) 1045-1054.

[53] A. Veksha, W. Zaman, D. B. Layzell, J.M. Hill. Enhancing biochar yield by co-pyrolysis of bio-oil with biomass: Impacts of potassium hydroxide addition and air pretreatment prior to co-pyrolysis, Bioresour. Technol. 171 (2014) 88-94.

[54] S. Hayashi, H. Amano, T. Niki, M. Yokota, K. Mae. A New Pyrolysis of Metal Hydroxide-Mixed Waste Biomass with Effective Chlorine Removal and Efficient Heat Recovery, Ind. Eng. Chem. Res. 49 (2010) 11825-11831.

[55] F. M. Pellera, E. Gidarakos, Effect of dried olive pomace – derived biochar on the mobility of 2 cadmium and nickel in soil, J. Environ. Chem. Eng. 3 (2015) 1163-1176..

[56] K. Zeng, D.P. Minh, D. Gauthier, E. Weiss-Hortala, A. Nzihou, G. Flamant, The effect of temperature and heating rate on char properties obtained from solar pyrolysis of beech wood, Bioresour. Technol. 182 (2015) 114-119.

[57] M.S. Hasan Khan Tushar, N. Mahinpey, A. Khan, H. Ibrahim, P. Kumar, R. Idem, Production, characterization and reactivity studies of chars produced by the isothermal pyrolysis of flax straw, Biomass Bioenergy. 37 (2012) 97-105.

[58] J.S. Dennis, R.J. Lambert, A.J. Milne, S.A. Scott, A.N. Hayhurst, The kinetics of combustion of chars derived from sewage sludge, Fuel. 84 (2005) 117-126.

[59] Y. Zhao, et al., Effect of pyrolysis temperature on char structure and chemical speciation of alkali and alkaline earth metallic species in biochar, Fuel Process. Technol. (2015), http://dx.doi.org/10.1016/j.fuproc.2015.06.029.

[60] S.Y. Zhang, J.P. Cao, T. Takarada. Effect of pretreatment with different washing methods on the reactivity of manure char, Bioresour. Technol. 101 (2010) 6130-6135.

Table 1

Proximate, elemental and XRF analyses of RDF.

Proximate (wt %)	
Ash	59.9 ± 1.4
Moisture	17.4 ± 1.6
Volatile Matter	18.8 ± 1.1
Fixed Carbon	3.90 ± 0.85
Elemental (wt %, daf basis)	
C	47.6 ± 0.62
H	5.31 ± 0.05
N	2.12 ± 0.02
S	0.38 ± 0.01
Inorganic matter (wt % of ash)	
SiO_2	37.4
CaO	30.8
Al_2O_3	5.91
Na_2O	4.31
Fe_2O_3	4.18
SO_3	3.82
K_2O	3.34
MgO	3.26
P_2O_5	3.16
Cl	2.02
TiO_2	0.695
PbO	0.213
BaO	0.161
ZnO	0.147
SrO	0.129
CuO	0.106
MnO	0.0922
ZrO_2	0.0607
Cr_2O_3	0.0588
NiO	0.0234
I	0.0227
SnO_2	0.0177
V_2O_5	0.0134
Ag_2O	0.0130

Table 2

Matrix of the factorial design adopted to analyze the pyrolysis behavior of RDF.

Level	Factors	
	x_1	x_2
	Peak temperature, T_{peak} (°C)	Heating rate, β (°C min^{-1})
Low (−1)	400	5
Middle (0)	500	22.5
High (+1)	600	40
Run	Factors	
	x_1	x_2
1	0	0
2	+1	−1
3	+1	+1
4	−1	−1
5	0	0
6	−1	+1
7	0	0

Table 3

Results of the design of experiments adopted to analyze the pyrolysis behavior of RDF.

Run	y_{char}	y_{FC}	H:C molar ratio	O:C molar ratio	S_{BET} $(m^2\,g^{-1})$	S_{mic} $(m^2\,g^{-1})$	d_{avg} (nm)	S_{tot} $(m^2\,g^{-1})$
1	0.7723	0.2273	0.1808	0.9145	15.0	2.04	8.47	12.4
2	0.7620	0.2768	0.1193	0.8069	18.7	6.65	7.02	7.80
3	0.7819	0.3108	0.0439	0.3472	24.8	11.1	5.63	8.98
4	0.8348	0.1724	0.5377	0.8420	6.20	n.d.[a]	12.2	12.7
5	0.7720	0.2387	0.1628	0.8800	14.6	1.99	8.36	12.3
6	0.8431	0.1389	0.2277	0.9097	10.1	n.d.[a]	10.8	5.23
7	0.8000	0.2104	0.1810	0.8310	16.6	2.59	8.44	12.4

[a] Not determined because S_{ext} was higher than S_{BET}.

Table 4

Summary statistics for the regression models based on the data given in Table 3 (values in brackets correspond to the *p-values* resulting from the hypothesis tests).

Response	β_0	β_1	β_2	β_{12}	Curvature[b]	R^2_{adj} [c]
y_{char}	0.8055	–0.0335	0.0071	0.0029	–0.0240	0.7509
		(0.048)	(0.473)	(0.753)	(0.190)	
y_{FC}	0.2247	0.0691	0.0001	0.0169	0.0007	0.9410
		(0.010)	(0.988)	(0.141)	(0.952)	
Molar H:C ratio	0.2322	–0.1505	–0.0963	0.0586	–0.0573	0.9956
		(0.001)	(0.003)	(0.008)	(0.019)	
Molar O:C ratio	0.7264	–0.1494	–0.0980	–0.1318	0.1487	0.9557
		(0.019)	(0.043)	(0.024)	(0.043)	
$S_{BET}\ (m^2\ g^{-1})$	14.938	6.788	2.488	0.5375	0.4625	0.9675
		(0.006)	(0.044)	(0.422)	(0.630)	
$d_{avg}\ (nm)$	8.915	–2.590	–0.715	0.020	–0.492	0.9993
		(0.000)	(0.002)	(0.555)	(0.008)	
$S_{tot}\ (m^2\ g^{-1})$	8.677	–0.287	–3.572	2.163	3.673	0.9993
		(0.019)	(0.001)	(0.000)	(0.000)	

[b] Regression coefficient for the overall curvature term.

[c] Calculated for the regression model that includes the curvature term.

Table 5

Pearson's correlation matrix for selected response variables (values in brackets correspond to the *p-values* obtained from the hypothesis tests) related to the potential stability of TPOMW-derived chars produced using the fixed-bed reactor.

	y_{FC}	*Fixed carbon content (wt %, af basis)*	*H:C molar ratio*
Fixed carbon content	0.266 (0.525)		
H:C molar ratio	–0.009 (0.984)	–0.898 (0.002)	
O:C molar ratio	–0.331 (0.424)	–0.931 (0.001)	0.882 (0.004)
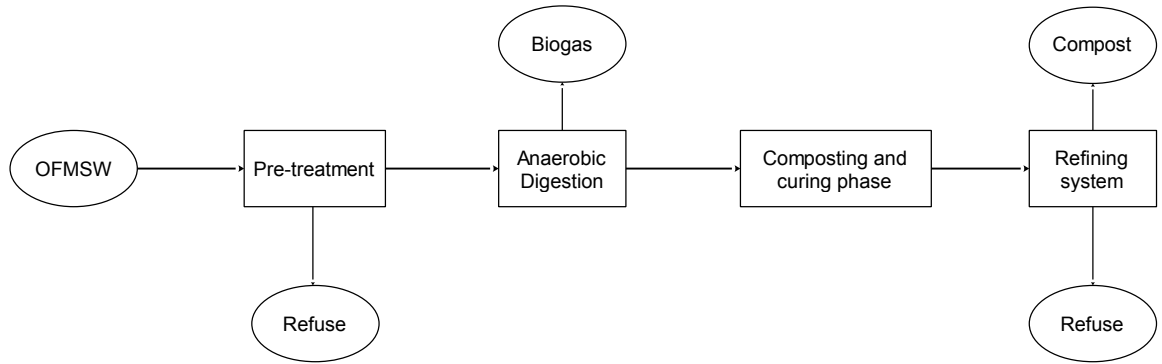
1

2

3

4

5

6

7

8

9

10

11

12

13

14

15

16

17

18

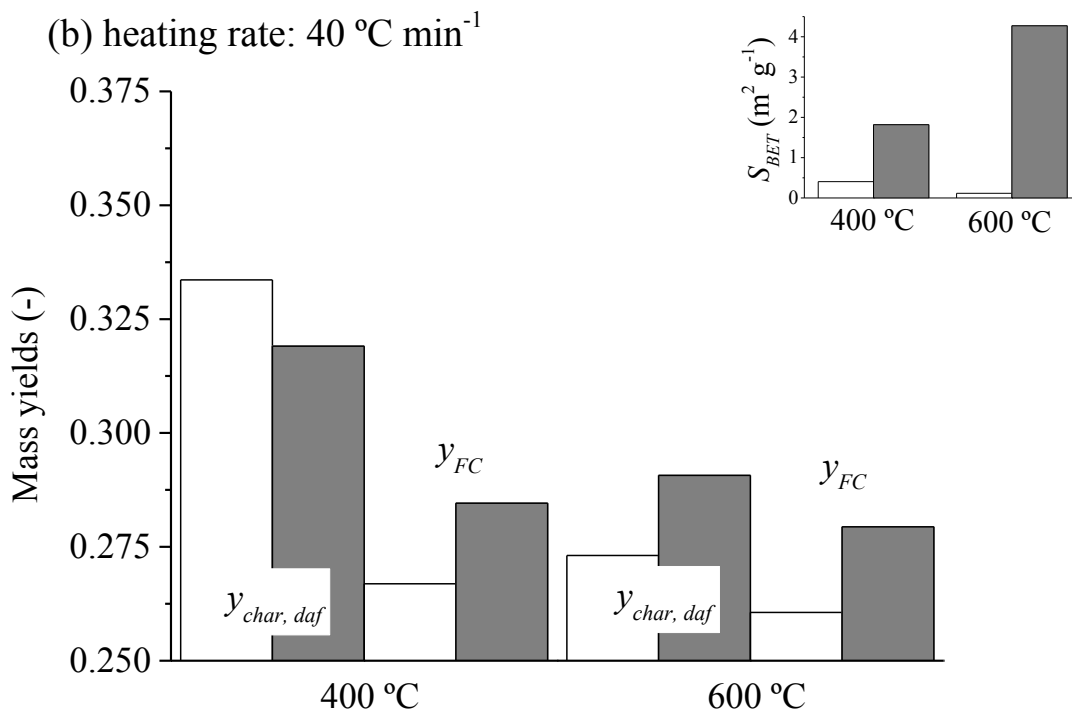19 **Fig. 1**. Simplified flowchart of a combined anaerobic/aerobic treatment of OFMSW.

20

The y-axis is labeled $(-1/\beta)\ (dm_{af}/dt)$ [°C^{-1}] and the x-axis is labeled Temperature [°C].

Legend:
- T_{peak} = 400 °C; β = 5 °C min^{-1}
- T_{peak} = 400 °C; β = 40 °C min^{-1}
- T_{peak} = 600 °C; β = 5 °C min^{-1}
- T_{peak} = 600 °C; β = 40 °C min^{-1}
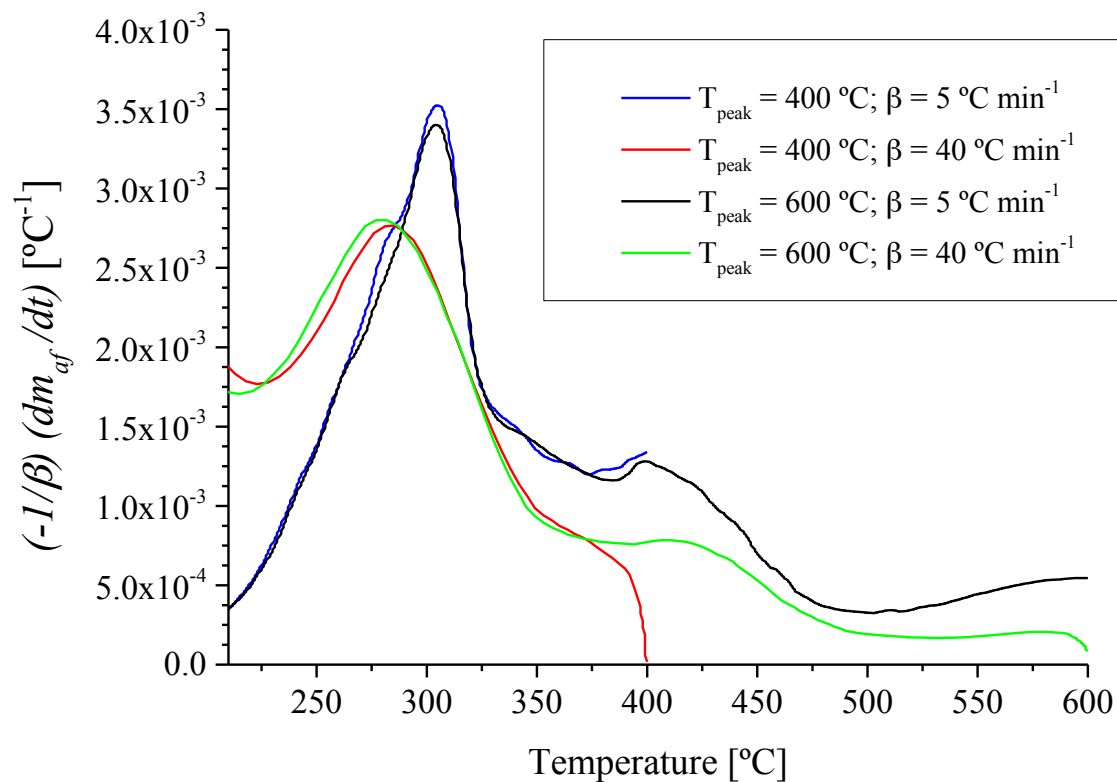
Fig. 2. Pyrolysis behavior of RDF as a function of both the peak temperature and heating rate factors.
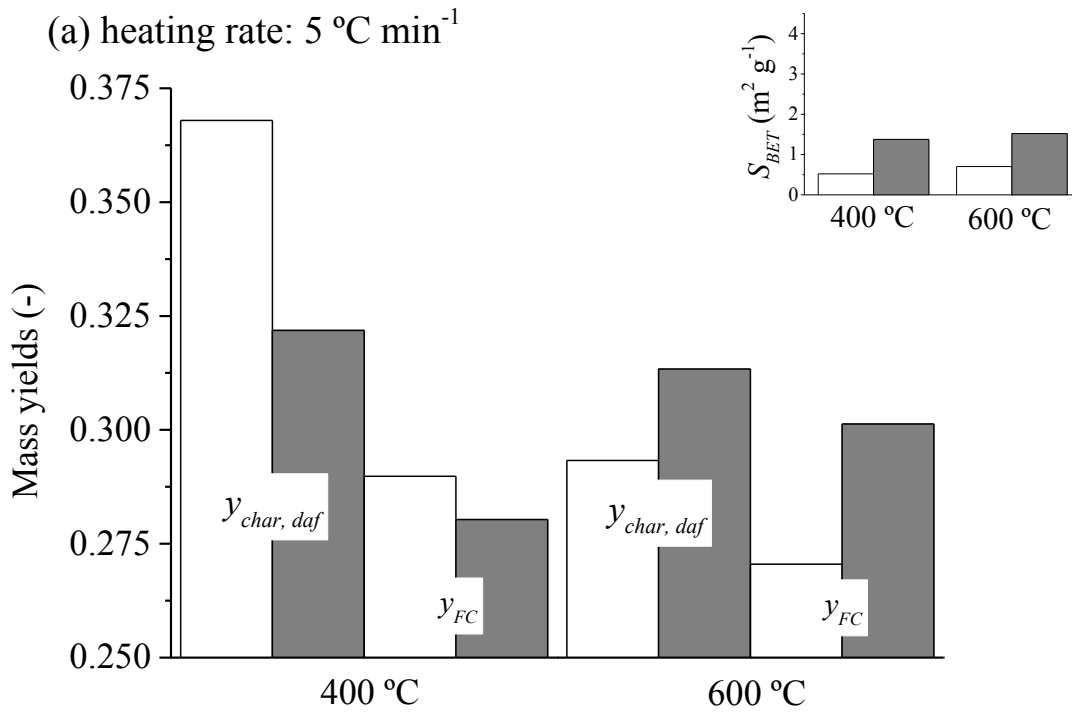
Fig. 3. Effect of RDF addition on char yield, fixed-carbon yield and surface area. White columns correspond to pyrolysis of TPOMW whereas gray columns represent pyrolysis of TPOMW-RDF mixtures (10% wt. of RDF).
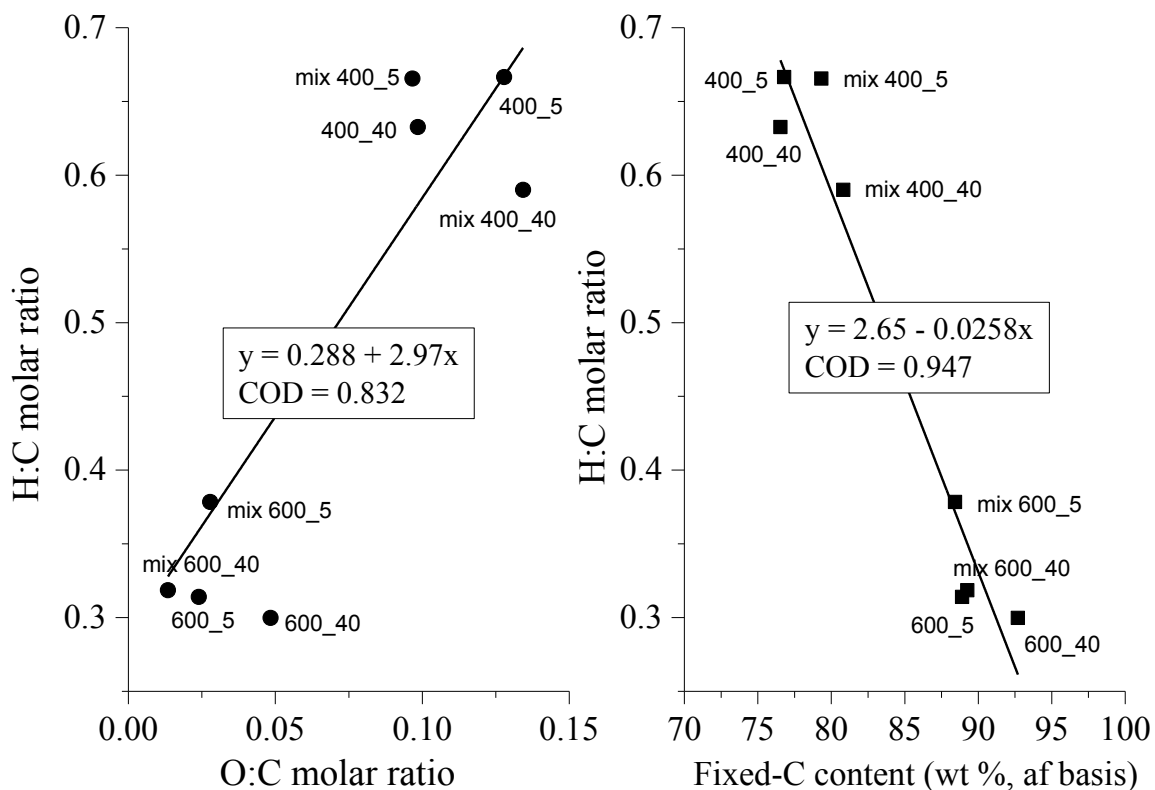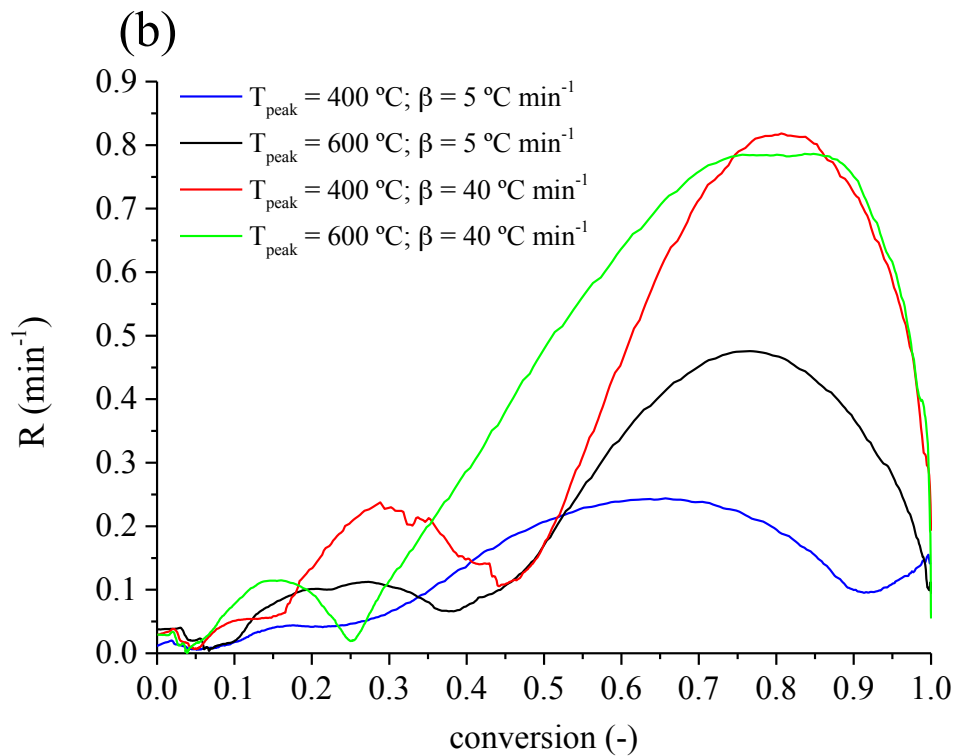
Fig. 4. Relationships between O:C and H:C molar ratios (on left) and fixed-carbon content and H:C molar ratio (on right) for TPOMW-derived chars produced using the fixed-bed reactor. Data point labels indicate peak temperature (400 or 600 °C) and heating rate (5 or 40 °C min^{-1}); the chars produced from TPOMW-RDF mixtures are designated by the term "mix".
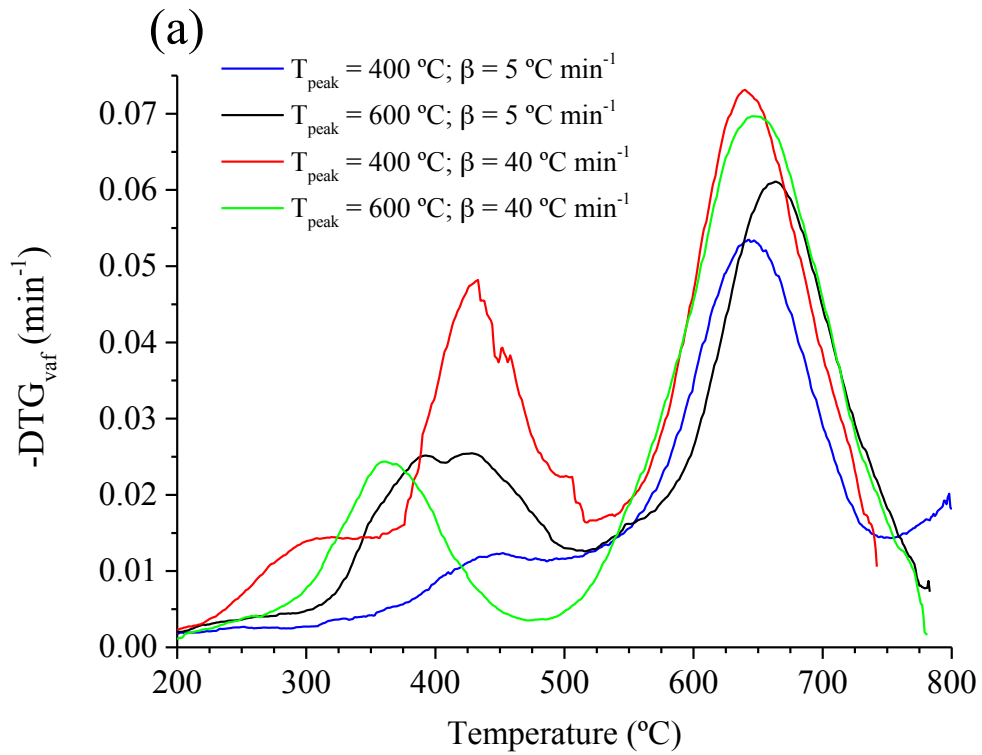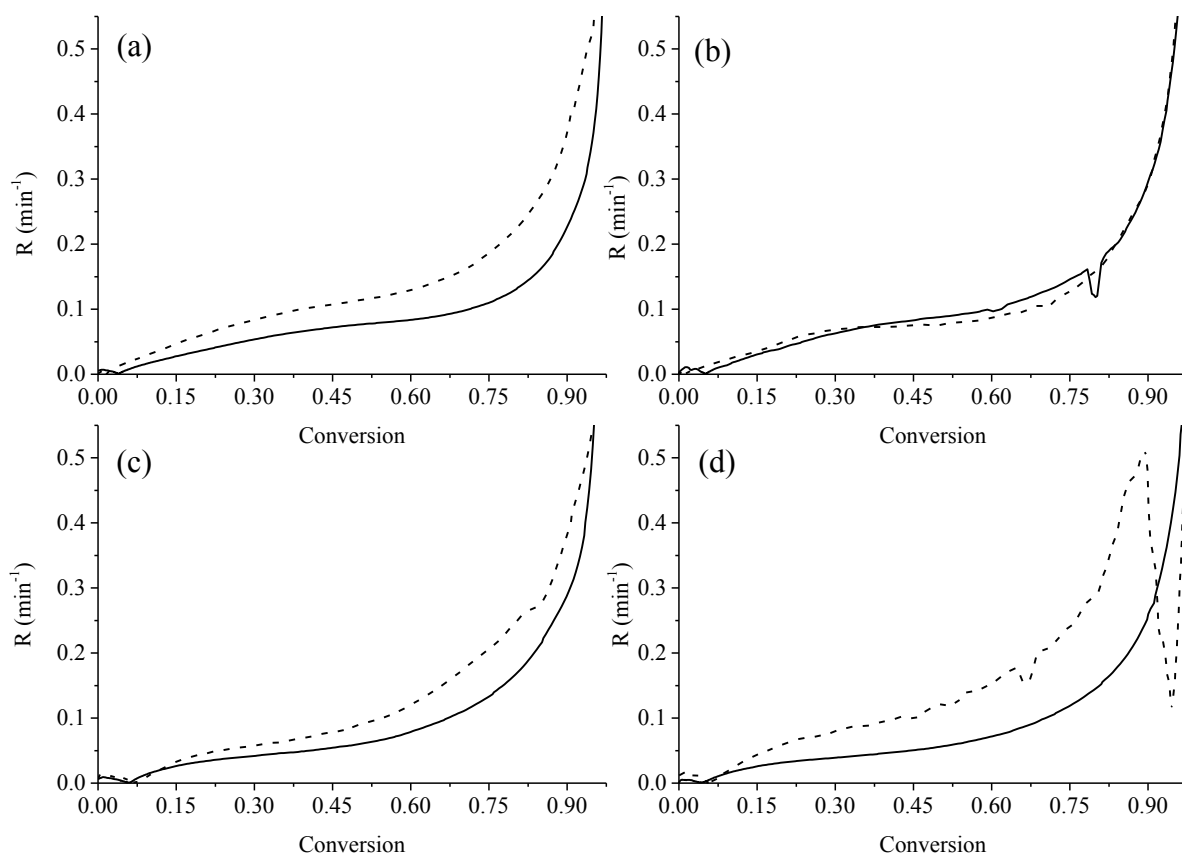
Fig. 5. (a) Combustion behavior and (b) reactivity of RDF-derived chars.

Fig. 6. Specific reactivity in air of the char samples (solid lines, from TPOMW; dashed lines, from TPOMW-RDF mixtures) as a function of char conversion and pyrolysis conditions: (a) 400 °C and 5 °C min^{-1}, (b) 400 °C and 40 °C min^{-1}, (c) 600 °C and 5 °C min^{-1}, and (d) 600 °C and 40 °C min^{-1}.